UC Davis

UC Davis Previously Published Works

Title

Disulfide-crosslinked nanomicelles confer cancer-specific drug delivery and improve efficacy of paclitaxel in bladder cancer

Permalink

https://escholarship.org/uc/item/9p9028q1

Journal

Nanotechnology, 27(42)

ISSN

0957-4484

Authors

Pan, Amy
Zhang, Hongyong
Li, Yuanpei
et al.

Publication Date

2016-10-21

DOI

10.1088/0957-4484/27/42/425103

Peer reviewed

eScholarship.org Powered by the California Digital Library
University of California

IOPscience iopscience.iop.org

Home Search Collections Journals About Contact us My IOPscience

Disulfide-crosslinked nanomicelles confer cancer-specific drug delivery and improve efficacy of paclitaxel in bladder cancer

This content has been downloaded from IOPscience. Please scroll down to see the full text.

2016 Nanotechnology 27 425103

(http://iopscience.iop.org/0957-4484/27/42/425103)

View the table of contents for this issue, or go to the journal homepage for more

Download details:

IP Address: 152.79.21.137
This content was downloaded on 19/02/2017 at 01:25

Please note that terms and conditions apply.

You may also be interested in:

Antitumor activity and systemic effects of PVM/MA-shelled selol nanocapsules in lung adenocarcinoma-bearing mice
Ludmilla Regina de Souza, Luis Alexandre Muehlmann, Lívia Carneiro Matos et al.

Combination chemotherapy of doxorubicin, all-trans retinoic acid and low molecular weight heparin based on self-assembled multi-functional polymeric nanoparticles
Ting Zhang, Hui Xiong, Fatima Zohra Dahmani et al.

pH-Responsive polymer-drug conjugates as multifunctional micelles for cancer-drug delivery
Yang Kang, Wei Ha, Ying-Qian Liu et al.

Bioconjugated PLGA-4-arm-PEG branched polymeric nanoparticles as novel tumortargeting carriers
Hong Ding, Ken-Tye Yong, Indrajit Roy et al.

Phenylboronic acid-decorated gelatin nanoparticles for enhanced tumor targeting and penetration
Xin Wang, Bing Wei, Xu Cheng et al.

A multi-functional nanoplatform for tumor synergistic phototherapy
Huijuan Zhang, Xiaojing Jiao, Qianqian Chen et al.

Multi-targeted inhibition of tumor growth and lung metastasis by redox-sensitive shell crosslinked micelles loading disulfiram
Xiaopin Duan, Jisheng Xiao, Qi Yin et al.

Improving anticancer activity and reducing systemic toxicity of doxorubicin byself-assembled polymeric micelles
MaLing Gou, HuaShan Shi, Gang Guo et al.

OPEN ACCESS
IOP Publishing
Nanotechnology

Nanotechnology **27** (2016) 425103 (9pp)
doi:10.1088/0957-4484/27/42/425103

Disulfide-crosslinked nanomicelles confer cancer-specific drug delivery and improve efficacy of paclitaxel in bladder cancer

Amy Pan[1,6,7], Hongyong Zhang[2,6], Yuanpei Li[1], Tzu-yin Lin[2], Fuli Wang[2,8], Joyce Lee[2], Mingshan Cheng[3], Marc Dall'Era[4], Tianhong Li[2,5], Ralph deVere White[4], Chong-Xian Pan[2,4,5] and Kit S Lam[1,2]

[1] Department of Biochemistry and Molecular Medicine, School of Medicine, University of California-Davis, Sacramento, CA 95817, USA
[2] Division of Hematology and Oncology, Department of Internal Medicine, School of Medicine, University of California-Davis, Sacramento, CA 95817, USA
[3] Jackson Laboratory, 4910 Raley Blvd, Sacramento, CA 95838, USA
[4] Department of Urology, University of California-Davis Cancer Center, Sacramento, CA 95817, USA
[5] VA Northern California Health Care System, 10535 Hospital Way, Mather, CA 95655, USA

E-mail: kslam@ucdavis.edu and cxpan@ucdavis.edu

Received 30 March 2016, revised 14 July 2016
Accepted for publication 16 August 2016
Published 19 September 2016

Abstract

Chemotherapy commonly used in the treatment of advanced bladder cancer is only moderately effective and associated with significant toxicity. There has been no appreciable improvement in overall survival over the last three decades. The goal of this project is to develop and characterize bladder cancer-specific nanometer-scale micelles loaded with the chemotherapeutic drug paclitaxel (PTX) and determine the anti-tumor activity and toxicity. Micelle-building-material telodendrimers were synthesized through the stepwise conjugation of eight cholic acid units at one terminus of polyethylene glycol (PEG) and a bladder cancer-specific targeting peptide named PLZ4 at the other terminus. To synthesize disulfide-crosslinked PLZ4 nanomicelles (DC-PNM), cysteine was introduced between the cholic acid and PEG. DC-PNM-PTX was synthesized through the evaporation method by loading PTX in the core. The loading capacity of PTX in DC-PNM was 25% (W/W). The loading efficiency was over 99%. DC-PNM-PTX was spherical with the median size of 25 nm. The stability of DC-PNM-PTX was determined in a solution containing sodium docecyl sulfate (SDS). It was stable in a SDS solution, but dissolved within 5 min after the addition of glutathione at the physiological intracellular concentration of 10 mM. *In vivo* targeting and anti-tumor activity were determined in immunodeficient mice carrying patient-derived bladder cancer xenografts (PDXs). After intravenous administration, DC-PNM specifically targeted the bladder cancer PDXs, but very little to the lung cancer xenografts in the same mice ($p < 0.001$). DC-PNM loaded with PTX overcame cisplatin

[6] These two authors contributed equally to this article.
[7] Current address: Department of Psychology, University of California San Diego, La Jolla, CA, USA.
[8] Current address: Department of Urology, The Four Military Medical School, Xi'an, People's Republic of China.

Original content from this work may be used under the terms of the Creative Commons Attribution 3.0 licence. Any further distribution of this work must maintain attribution to the author(s) and the title of the work, journal citation and DOI.

 © 2016 IOP Publishing Ltd Printed in the UK

resistance, and improved the median survival from 55 d with free PTX to 69.5 d ($p = 0.03$) of mice carrying PDXs. In conclusion, DC-PNM remained stable in the SDS solution, specifically targeted the bladder cancer xenografts *in vivo*, and improved the anti-cancer efficacy of PTX.

S Online supplementary data available from stacks.iop.org/NANO/27/425103/mmedia

Keywords: bladder cancer, nanomicelle, paclitaxel, targeted delivery

(Some figures may appear in colour only in the online journal)

Introduction

Bladder cancer is the 4th most common cancer in men and 12th in women [12]. It is estimated that approximately 77 000 new cases will be diagnosed in the United States in 2016. Even though most of these cases are at the non-myoinvasive stage [1], it is the locally advanced and metastatic bladder cancers that cause almost all the mortalities. Platinum-based chemotherapy is an integrated therapeutic modality in the management of these two groups of patients. At the setting of neoadjuvant chemotherapy for locally advanced cancer, less than 40% of patients achieve complete remission (no viable cancer cells) at the time of cystectomy and enjoy an 85% five-year overall survival rate, compared to only a 35% five-year survival rate of the remaining 60% of patients who still have viable cancer cells after neoadjuvant chemotherapy [3]. For metastatic bladder cancer, the most commonly used MVAC (methotrexate, vinblastine, doxorubicin/Adriamycin and cisplatin) and GC (gemcitabine and cisplatin) regimens have a response rate of approximately 50% [16]. In cases of disease progression or recurrence, even though several medications are commonly used in clinic, there is no standard second-line therapy approved by the US Food and Drug Administration. Paclitaxel (PTX) is one of the drugs commonly used as salvage chemotherapy with a response rate around 20% [15]. PTX is highly hydrophobic and is dissolved in Cremophor EL/ethanol (Taxol®) for clinical application. Hence, it is sometimes associated with severe allergic reactions, mainly due to the solvent, even with steroid and anti-histamine pre-chemotherapy medications. The prognosis of bladder cancer has not changed significantly over the last three decades [11]. Therefore, there is a great need to improve treatment for more effective outcomes.

We previously reported the development of multi-functional nanometer-scale micelles that can be loaded with hydrophobic therapeutic and diagnostic drugs [4, 6, 7, 17]. The micelle-building polymer telodendrimers are composed of a polyethylene glycol (PEG) backbone conjugated with dendritic octamers of cholic acid at one terminus of the PEG. In aqueous solution with hydrophobic drugs, telodendrimers can self-assemble into nanometer-scale micelles in which the amphiphilic cholic acid forms the core to load hydrophobic drugs.

Even though these micelles showed promising cancer-specific targeting and toxicity profile, one major drawback of these micelles is that the building-material telodendrimers are held together through hydrophobic forces. After intravenous administration, the mechanical force of blood circulation and detergent effect of lipoproteins can break up these micelles and prematurely release the drug load. In addition, telodendrimers work as a detergent and can cause hemolysis after intravenous administration. To overcome these potential drawbacks, disulfide-crosslinked micelles were developed [5]. In these micelles, cysteine is introduced into the telodendrimers. After the telodendrimers form micelles, cysteines from the adjacent telodendrimers form disulfide bonds that covalently hold the telodendrimers together and stabilize the micelles during blood circulation. Upon entrance into target cells, the disulfide bonds can be reduced, open under the reducing intracellular environment, and release the drug load inside the target cells.

Here, we report the development of disulfide-crosslinked PLZ4-nanomicelle (DC-PNM) that can specifically target bladder cancer cells. To synthesize bladder cancer-targeting micelles, the other terminus of PEG is conjugated with a bladder cancer-specific ligand named PLZ4 (amino acid sequence: cQDGRMGFc—upper case letters represent L-amino acids and lower case letters represent unnatural D-cysteines used to cyclize and stabilize the peptide) [19]. During drug loading and the formation of micelles, hydrophilic PEG and PLZ4 are exposed on the surface for cancer-specific drug delivery. DC-PNM withstood the detergent effect of a strong ionic detergent sodium dodecyl sulfate (SDS), while being able to be reduced and release the drug load under the physiological concentration of glutathione. At the same dose, DC-PNM-PTX was more effective than free PTX in Cremophor EL/ethanol.

Materials and methods

Synthesis and characterization of PLZ4 and micelles, and loading of imaging and chemotherapeutic agents in micelles

Both PLZ4 (amino acid sequence: cQDGRMGFc) and thiolated telodendrimers (named as PEG^{5k}-Cys_4-L_8-CA_8) were synthesized and characterized (chemical structure, purity, and cholic acid conjugation) as previously described [5, 8, 17]. In brief, dendritic octamers of cholic acid were conjugated to linear PEG via solution-phase condensation reactions. To synthesize targeting PLZ4 nanomicelles in which 50% of non-thiolated telodendrimers (PEG^{5K}-CA_8) were conjugated to PLZ4, an aqueous-phase 'click chemistry' catalyzed by cuprous ion was used to couple the alkyne group on PLZ4 peptides to the azide group at the end of PEG on the telodendrimer at a molar ratio of 1:2 (PLZ4: PEG) [14]. After conjugation, no free PLZ4 was detected as determined by high-performance liquid chromatography (HPLC) after

ultracentrifugation with a 3KMWSO filter (Millipore, Billerica, MA), suggesting PLZ4 had been successfully conjugated to the telodendrimers. The conjugation was further confirmed with proton nuclear magnetic resonance (^{1}H-NMR).

To load PTX or fluorescent dye DiD (Invitrogen, Carlsbad, CA) into the micelles, PTX/DiD and telodendrimer (20 mg) were dissolved in chloroform (5 ml) in a 10 ml flask. Chloroform was removed on a rota-evaporator under vacuum, then 1 ml of USP (US Pharmacopeia) saline was added and the mixture was vortexed and sonicated for 30 min at room temperature. The PTX-loaded micelles were then crosslinked via O_2-mediated oxidation as described previously [5]. It was sterilized using a filter (0.22 μm) and stored at 4 °C for further study. After self-assembly, the more hydrophilic PLZ4 ligands were displayed on the surface of the micelles.

The final product was analyzed for drug loading capacity and encapsulating efficiency using HPLC. The area under the curve of the PTX peak was measured and the calibration curve was generated. The encapsulating efficiency was calculated using drug loading observed from calibration*100%/ actual amount of drug originally washed, and micelle size and dispersion were evaluated with a dynamic light scattering (DLS) particle sizer and transmission electron microscopy (TEM). To determine the stability, the DC-PNM was incubated with SDS at 2.5 mg ml^{-1}, followed by the addition of glutathione at the physiological concentration of 10 mM. The size of DC-PNM was then determined by DLS.

In vivo xenograft imaging study

In all animal studies in this study, the animal protocols were approved by the Jackson Laboratory (JAX) Institutional Animal Care and Use Committee (IACUC, Protocol No. 12027) and the UC Davis IACUC (Protocol No. 17794). Patient-derived xenografts were developed from unselected uncultured clinical patient specimens as previously described [10]. To compare *in vivo* drug delivery, human non-small cell lung cancer cell line, H23, was planted at the right lower flank as a negative control to determine the background DC-PNM delivery to xenografts as PLZ4 does not bind to H23 cells, and a patient-derived bladder cancer xenograft BL-0645 was planted at the left flank of NOD/SCID interleukin-2 receptor gamma-deficient (NSG) mice (The Jackson Laboratory, Bar Harbor, MN). The NSG mice were used because of the immunodeficient status associated with a high engraftment rate of patient-derived xenografts. When the tumor xenografts reached 0.5–1.0 cm, the mice (three mice per group) were injected with 100 μl of DC-PNM loaded with DiD/PTX and whole-body imaging was acquired at 5, 15, and 30 min, 2, 8 and 24 h after dosing. The mice were then sacrificed at 24 h. Tumors and major organs were harvested for *ex vivo* imaging study. Imaging was processed, quantified and analyzed by Kodak imaging software (Kodak).

Therapeutic efficacy and toxicity study in a subcutaneous xenograft model in mice

To evaluate the anti-cancer efficacy and toxicity of DC-PNM loaded with PTX, NSG mice bearing cisplatin-resistant patient-derived xenografts BL0293 were used for this study. When the tumor size reached 150–200 mm^3, eight mice per group were treated with phosphate-buffered solution (PBS) control, cisplatin at 2 mg kg^{-1}, free PTX and DC-PNM-PTX, both at 10 mg kg^{-1}. A total of six doses for each treatment group was given intravenously every 3–4 d. Another set of Balb/c mice was treated with the same dose and schedule to determine the toxicity. Tumor size was measured every 3–4 d and calculated using the formula: 0.5 × length × width^2 (mm^3). Body weight, appetite, hair coat and activity were monitored regularly. When the tumors reached the 1500 mm^3 tumor endpoint, the animals were euthanized for humane reasons. Blood was drawn 3 d after the fourth dose for blood counts, liver and kidney function tests. Another group of mice was sacrificed after the fourth dose of each treatment. Vital organs and tumors were harvested for histopathological evaluation.

Statistics

The experiments were repeated at least in triplicate. The mean values and standard deviation were presented for each set of experiments. For the determination of micelle delivery to tumor sites, we calculated mean fluorescence intensities of the tumor area and of the normal tissue area by means of the region-of-interest function using Kodak Image Analysis Software (Kodak), then plotted a pseudocolored scale based on the semiquantitative information from near-infrared fluorescence images by integrating fluorescence intensities from equal areas within the tumor and normal tissue regions. One-way ANOVA analysis was used for statistics. A P value less than 0.05 was considered as significant.

Results

Characterization and stability assay

We synthesized DC-PNM in which the PLZ4 ligand density on the surface was 50% as the molar ratio of PLZ4 to the telodendrimers was 1:2 during the conjugation with 'click chemistry', and no free PLZ4 was detected after conjugation. To synthesize DC-PNM loaded with PTX (DC-PNM-PTX), various ratios of PTX and telodendrimer/PLZ4-telodendrimer were tried. The loading capacity was 5–10 mg ml^{-1} for PTX in 20 mg ml^{-1} of the telodendrimers. In this report, we used DC-PNM-PTX with the loading capacity of 25% (w/w of PTX/telodendrimer): PTX 5 mg/ml, and telodendrimer/PLZ4-telodendrimer: 20 mg ml^{-1}. The loading efficiency was over 99%, meaning over 99% of the PTX was loaded into DC-PNM. DC-PNM-PTX was spheric in shape as determined by TEM. The median size was around 25 nm (figure 1(b)). The size of DC-PNM-PTX was further confirmed with a DLS particle sizer that showed the size of 23 +/− 6 nm (figure 1(c)).

Stability of DC-PNM-PTX in the SDS solution

To determine the stability, DC-PNM-PTX was incubated in PBS containing 2.5 mg ml^{-1} of a strong ionic detergent SDS. Unlike previous studies showing that non-crosslinked

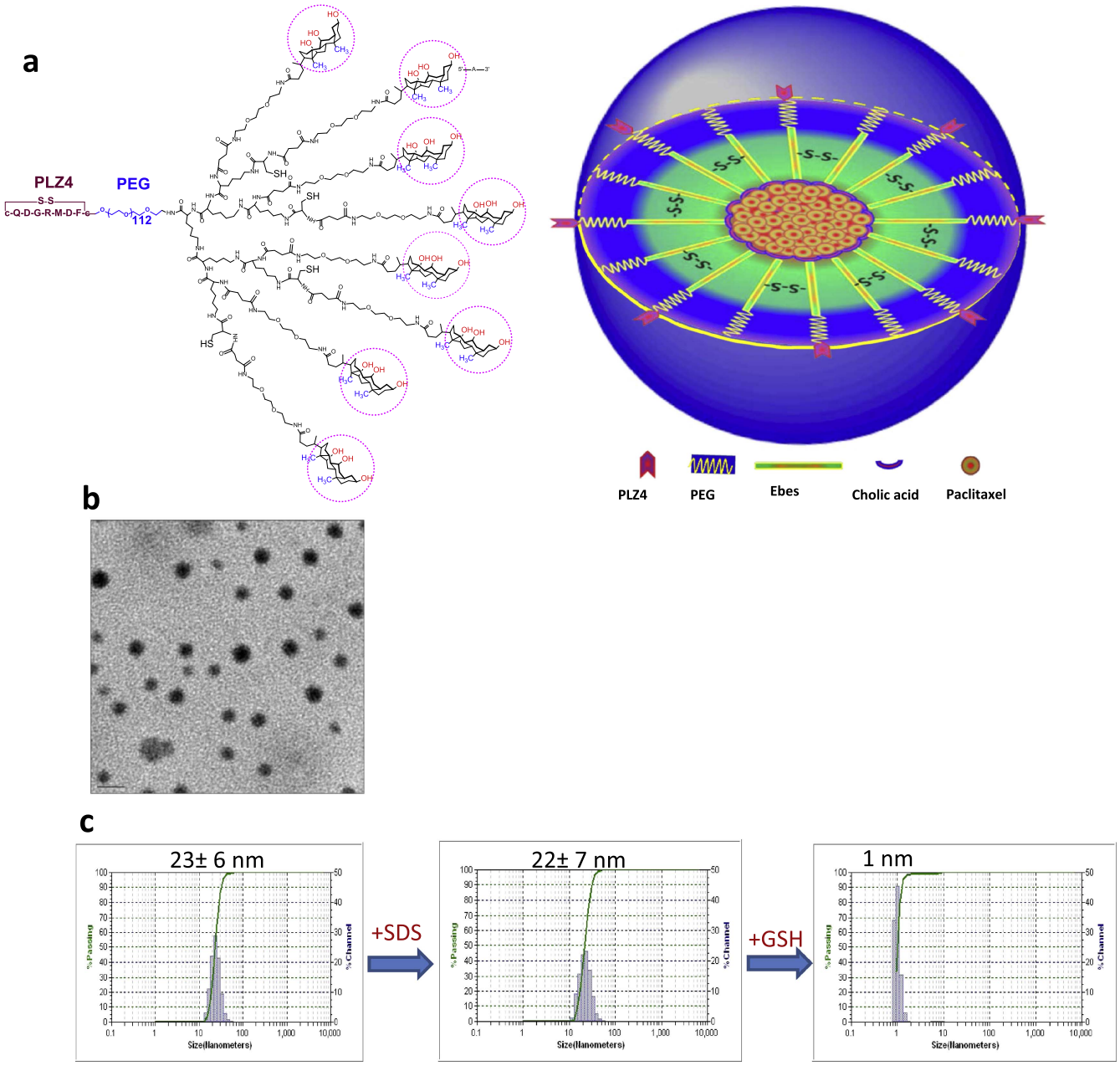

Figure 1. Characterization of DC-PNM. (a) **Schematic diagram of the chemical structure of the PLZ4-telodendrimer and DC-PNM.** Telodendrimer PEG^{5k}-CA_8 represents PEG with the molecular weight of 5000 daltons (PEG^{5k}) conjugated with eight cholic acid (CA_8) subunits through cysteine-Ebes linkers at one terminus. To synthesize DC-PNM, PLZ4 is conjugated at the other terminus of PEG in the telodendrimers. CA is an amphiphilic molecule with the hydrophobic methyl groups (blue) at one side and hydrophilic hydroxyl groups (red) at the other side. This facial amphiphilic structure allows the formation of hydrophobic spheric micelle core to load hydrophobic drugs, such as PTX, while leaving hydrophilic PEG and PLZ4 displayed on the surface for targeted drug delivery. The data presented here was obtained with DC-PNM in which 50% of the telodendrimers are conjugated with PLZ4. (b) **TEM examination of TDC-PNM**. DC-PNM with 50% crosslinking and loaded with PTX 4 mg ml^{-1} in 20 mg ml^{-1} of the telodendrimers were used for this study. The average size of the DC-PNM was around 25 nm. The scale bar: 50 nm. (c) **Stability of DC-PNM**: DC-PNM with 50% crosslinking and PTX 4 mg ml^{-1} was incubated in PBS (left panel), and in the presence of SDS at 2.5 mg ml^{-1} (middle panel). A DLS analysis was performed after 30 min of incubation, showing that DC-PNM remained stable in the SDS solution. It dissolved within 5 min after glutathione 10 mM was added (right). Left panel: in PBS; middle: in the SDS solution after incubation for 30 min; right: 5 min after the addition of glutathione at 10 mM.

nanomicelles immediately dissolved in the presence of SDS [5], DC-PNM-PTX was stable in the SDS solution (figure 1(C), middle panel). Within 5 min after the addition of a physiologically relevant concentration of glutathione at 10 mM [2], DLS analysis showed that the size of DC-PNM-PTX was reduced to around 1 nm (figure 1(c), right panel), suggesting that the crosslinked micelles were reduced; DC-PNM-PTX had disintegrated; and the drug load was released. Consistent with this finding, the half-life ($T_{1/2\beta}$) of PTX increased from 526.9 +/− 182.9 min with free PTX to 929.5 ± 134.8 min ($p = 0.037$) with DC-PNM-PTX after bolus intravenous injection of 10 mg kg^{-1} body weight (online supplementary information).

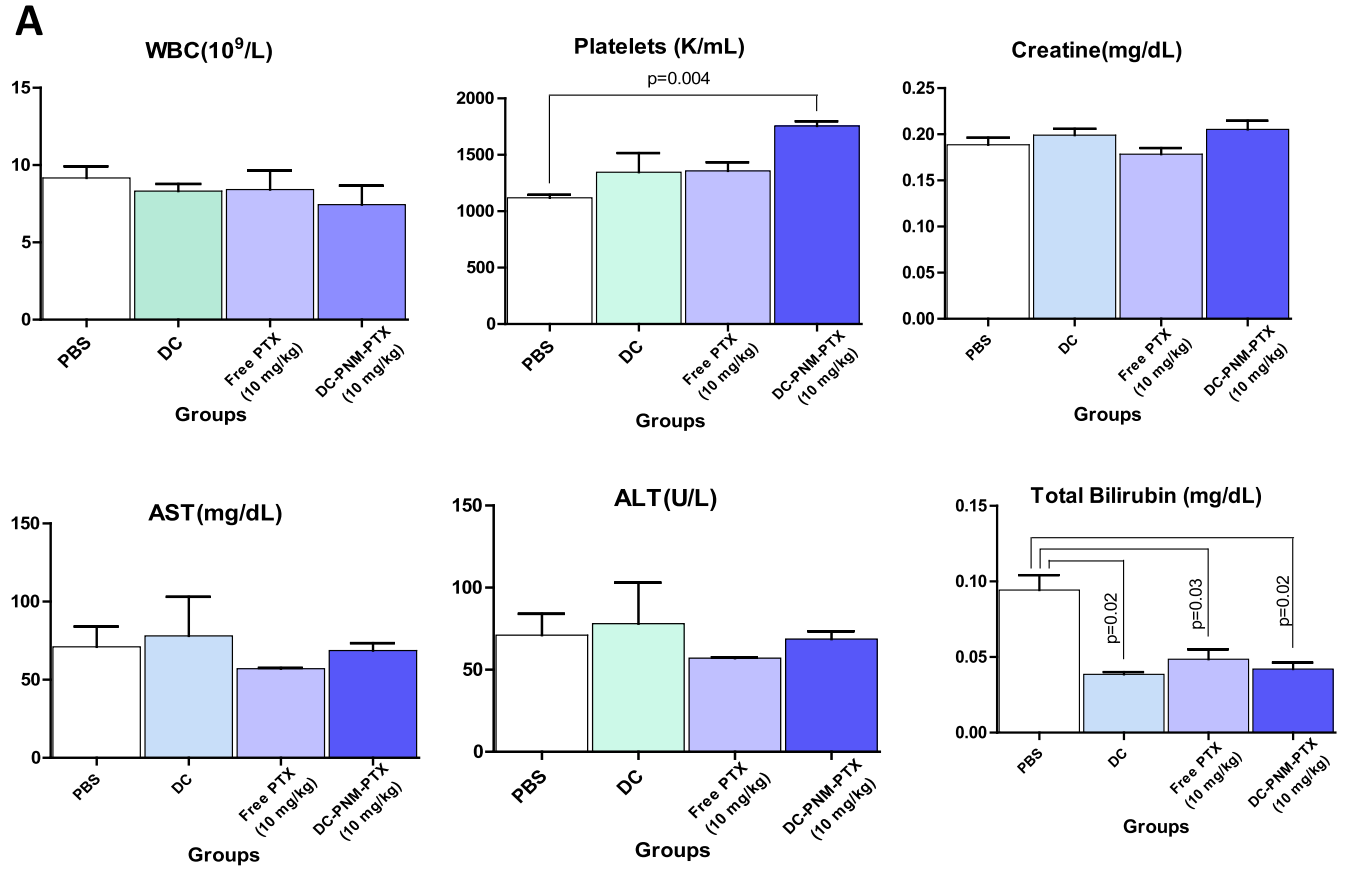

Figure 2. Blood counts, chemistry panel and histopathological examination of vital organs. (A) **Blood counts and chemistry panels.** Blood specimens were collected 3 d after the last dose of treatment. No significant changes in the blood counts, kidney (creatinine) and liver functions (AST, ALT and total bilirubin) were observed between treatment groups, except for a high platelet count in the group treated with DC-PNM-PTX and low bilirubin in all treatment groups. PBS: control; DC: DC-PNM without PTX loading; WBC: white blood cells; AST: aspartate transaminase; ALT: alanine transaminase. (B) **Histopathological examination of vital organs.** Cellular disarray with enlarged hepatocytes with loss of cell membrane, reactive nuclear vesicular chromatin, and vacuolar degeneration of the cytoplasm of hepatocytes were observed in the livers treated with free PTX or DC-PNM-PTX. No other significant changes were observed under light microscope (400× and 40×).

Drug toxicity

We next determined whether the formulation of PTX in DC-PNM would change the toxicity of PTX. Consistent with a previous study [18], treatment with PTX at 10 mg kg^{-1} was tolerated. All mice treated with free PTX or DC-PNM-PTX had slightly decreased activity, especially in the group treated with free PTX injection. Body weight remained stable or slightly decreased at comparable extents in all groups during treatment. No significant other toxicity was observed.

Blood tests were collected 3 d after the last dose. We did not observe any significant decrease in the white blood cell count, abnormal increase in liver function tests (aspartate aminotransferase (AST) and alanine aminotransferase (ALT)), or kidney function (creatinine level) (figure 2(A)). In fact, when compared to the PBS control, the platelet count slightly increased in the DC-PNM-PTX group ($p = 0.004$) while the total bilirubin decreased in the empty DC-PNM ($p = 0.02$), free PTX ($p = 0.03$) and DC-PNM-PTX ($p = 0.02$). Even though statistically significant, these differences were not likely clinically significant.

We also harvested the vital organs for histopathological examination under light microscope. Damage to hepatocytes was observed in the groups treated with free PTX and DC-PNM-PTX, characterized by cellular disarray with enlarged hepatocytes with loss of cell membrane, reactive nuclear vesicular chromatin, and vacuolar degeneration of the cytoplasm (figure 2(B) top row). No significant difference was observed between these two groups. No other visible histopathological changes were detected in any other groups.

In vivo cancer-specific drug delivery

We then determined whether PLZ4 on the surface of DC-PNM could guide the cancer-specific delivery of DC-PNM-PTX into bladder cancer xenografts. To strictly control other confounding factors, we established a xenograft from a non-small cell lung cancer cell line H23 at the right flank, and a patient-derived bladder cancer xenograft BL-0645 at the left flank in the same immunodeficient NSG mice. In this experiment, H23 was used as a negative control as PLZ4 does not bind to H23 cells. NSG mice were used because they have profound immunodeficiency

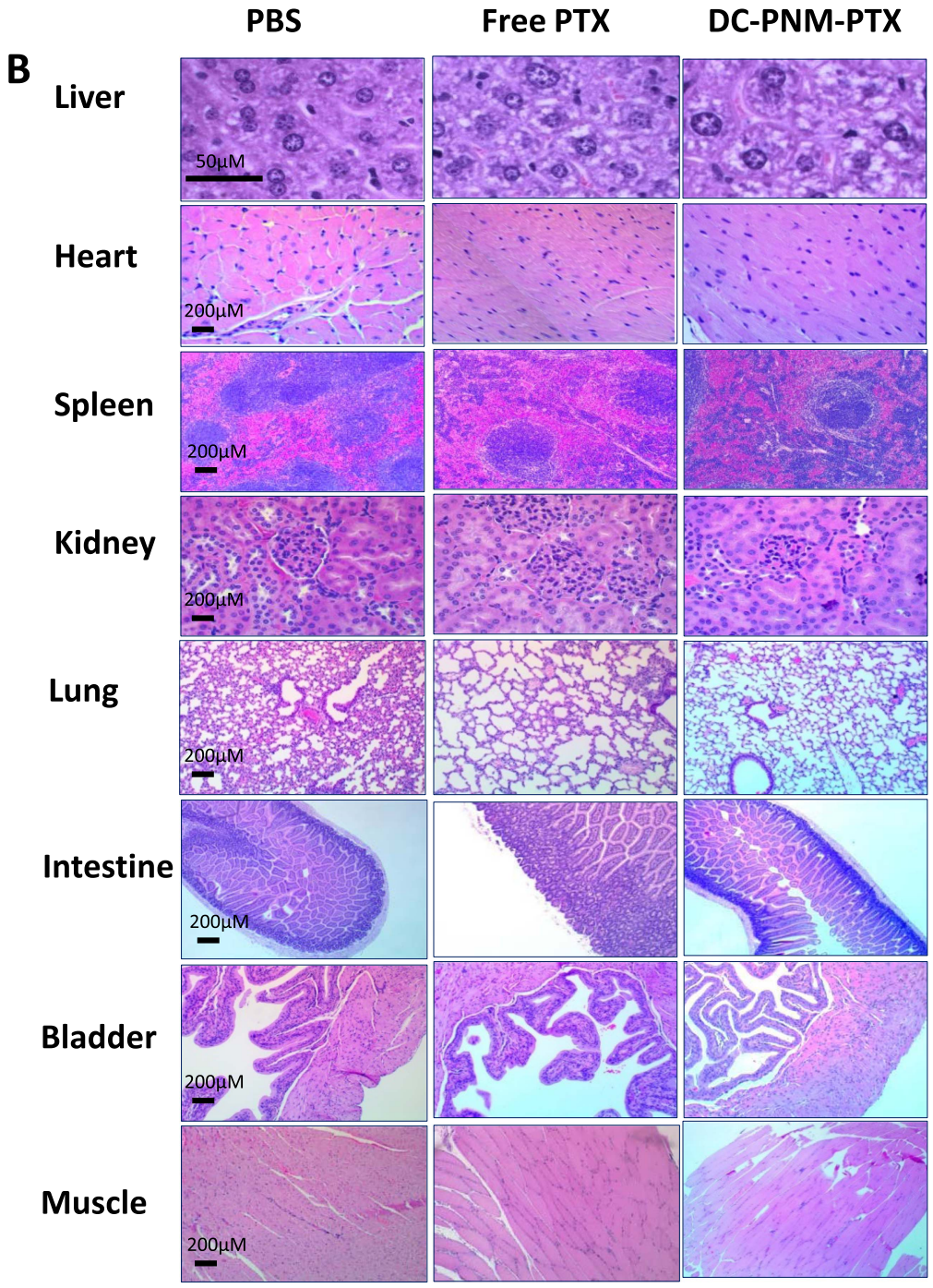

Figure 2. (Continued.)

that allows the establishment of patient-derived xenografts instead of using cell lines as in most other studies. Patient-derived bladder cancer xenografts were developed from unselected and uncultured clinical patient cancer specimens. We previously showed that these bladder cancer xenografts maintained their morphology fidelity and 92%–97% of the genetic alterations of the parental patient cancers [10]. Therefore, studies performed in patient-derived bladder cancer xenografts can more likely be translated into clinical application than xenografts from cell lines. After intravenous administration of DC-PNM co-loaded with DiD and PTX, a near-infrared signal was observed in both xenografts, possibly secondary to the small size of DC-PNM (<25 nm) and the enhanced permeability and retention (EPR) effect (figure 3(A)). However, a much stronger signal was observed in the bladder cancer xenografts BL-0645 than that in the lung cancer xenografts in the same mice. At 24 h, the near-infrared signal at the patient-derived xenograft BL-0645 was much higher than that at the xenografts from H23 (figures 3(B) and (C)): 45 255.1 +/− 707.5 versus 22 005.1 +/− 2383.2 ($p = 0.007$).

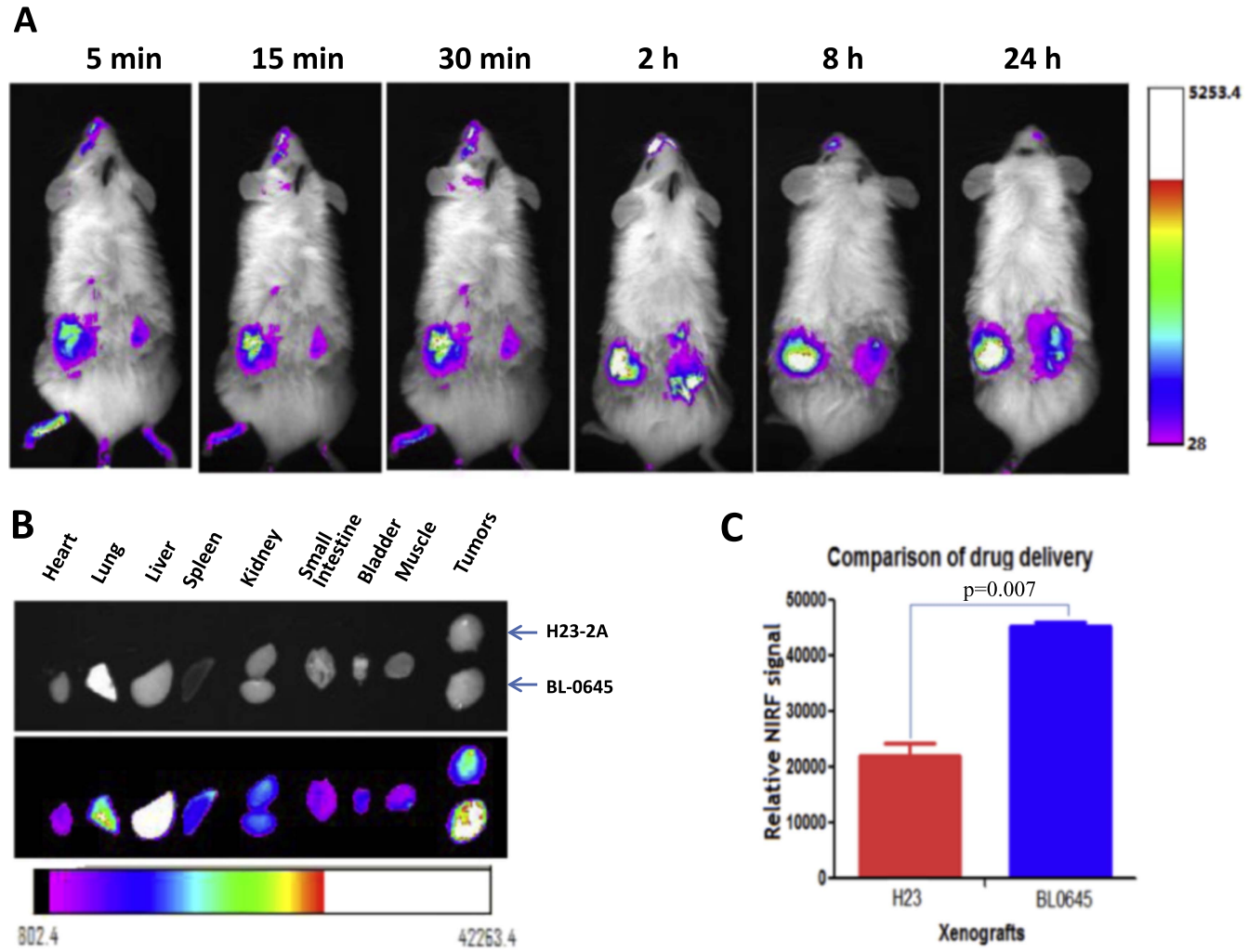

Figure 3. *In vivo* drug delivery of DC-PNM. (A) **Near-infrared fluorescence imaging.** NSG mice carrying a non-small cell lung cancer xenograft H23-2A at the right flank and a patient-derived bladder cancer xenograft BL-0645 at the left flank. DC-PNM co-loaded with PTX and a near-infrared fluorescence dye DiD was injected through the tail vein. White-light imaging and near-infrared imaging were taken and overlaid at 5, 15 and 30 min, 2, 8, and 24 h after dosing. Significantly more near-infrared signal was observed at the left flank overlaying the bladder cancer xenograft. (B) ***Ex vivo* imaging to determine drug delivery.** Tumor xenografts and vital organs were harvested 24 h after dosing. Significantly more fluorescence was observed in the bladder cancer xenograft BL-0645 than the non-small cell lung cancer xenograft H23-2A from the same mouse. The liver also had significant uptake, followed by moderate uptake in the lung. However, we did not observe anything abnormal in the liver function test. (C) **Comparison of drug delivery between lung and bladder cancer xenografts.** The near-infrared fluorescence (NIRF) signal was measured at the same area of non-small cell lung and bladder cancer xenografts. Much more fluorescence was observed in the bladder cancer xenografts BL-0645 than the lung cancer xenografts H23-2A: 45 255.1 +/− 707.5 versus 22 005.1 +/− 2.383.2 ($p = 0.007$), suggesting a cancer-specific drug delivery.

Improved anti-tumor efficacy with DC-PNM-PTX

Next, we determined whether improved drug delivery could be translated into improved anti-tumor efficacy (figure 4). In this experiment, we used a bladder cancer patient-derived xenograft BL0293 that is relatively resistant to cisplatin, one of the first-line drugs used in bladder cancer. First, we measured the treatment effect on tumor growth (figure 4(A)). In this experiment, we used ten times the baseline tumor size as the endpoint for tumor growth. Experiments were started when the tumor size was ~0.1–0.2 cm^3. Hence, ten times the baseline tumor size would be around 1–2 cm^3, the humane endpoint of euthanasia. The cisplatin moderately delayed the tumor growth, and increased the median time of the tumor growth to ten times the baseline from 12.9 d for the control group to 25.3 d with cisplatin ($p < 0.001$), while free PTX was very effective and delayed the tumor growth to 61.4 d, which was statistically significant ($p < 0.001$) when compared to both the control and cisplatin groups. DC-PNM-PTX further delayed tumor growth to 71.5 d ($p = 0.01$) when compared to the free PTX group (figure 4(A)).

Next, we determined whether the delay in tumor growth was translated into improvement of survival (figures 4(B) and (C)). Compared to the median survival of 23.5 d of the control group, cisplatin prolonged the survival to 39 d ($p < 0.001$). It was 55 d in the free PTX group, which is statistically significant ($p < 0.001$) when compared to both the control and cisplatin group. Compared to free PTX, DC-PNM-PTX further increased the median survival to 69.5 d ($p = 0.03$).

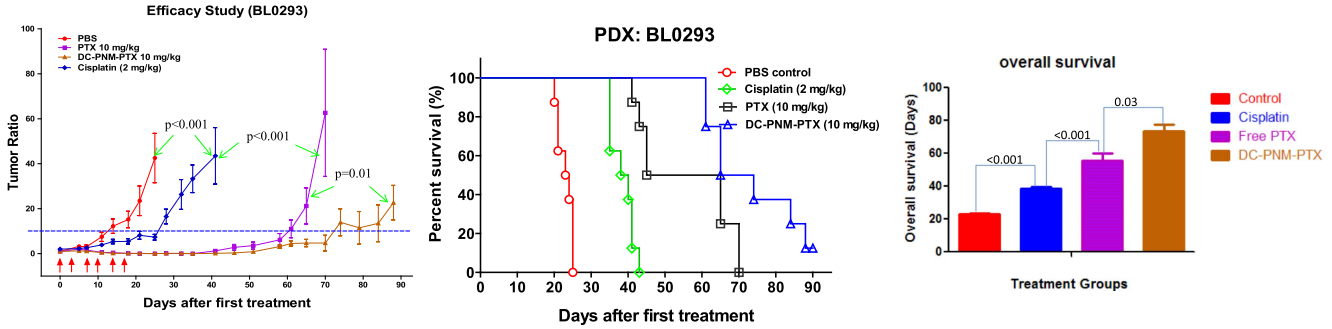

Figure 4. Comparison of anti-tumor activity. (A) **Tumor growth curves**. When the size of the tumor xenografts reached around 0.1–0.2 cm^3, the NSG mice carrying patient-derived bladder cancer xenografts were treated with PBS control, cisplatin 2 mg kg^{-1}, free PTX and DC-PNM-PTX with the PTX dose of 10 mg kg^{-1} in both groups. The treatment was administered through tail vein injection (red arrows) once every 3–4 d for a total of six doses per mouse. The tumor sizes were measured every 3–4 d. The tumor volume was calculated using the formula: 0.5 × length × $width^2$ (mm^3). The mice were euthanized when the tumor volume reached 1.5–2 cm^3. The median time of the tumor growth to ten times the baseline (10X BL) was 12.9 d for the PBS control and 25.3 d in the cisplatin group ($p < 0.001$). Compared to the PBS control and cisplatin, free PTX delayed the tumor growth to 10X BL by 61.4 d ($p < 0.001$ compared to both). Compared to free PTX, DC-PNM-PTX further delayed the tumor growth to 10X BL to 71.5 d ($p = 0.01$). (B) **Survival curve.** The NSG mice (seven mice per group) carrying patient-derived xenografts BL0293 were treated with PBS (control), cisplatin at 2 mg kg^{-1}, free PTX at 10 mg kg^{-1} and DC-PNM-PTX 10 mg kg^{-1} every 3–4 d for a total of six doses. The mice were sacrificed when the tumor volume reached 1.5 ~ 2.0 cm^3, or other humane endpoints, such as body weight loss of over 10%. (C) **Median survival and statistical analysis**. The median survival of the PBS control and cisplatin groups was 23.5 and 39, respectively ($p < 0.001$). Compared to the PBS and cisplatin groups, free PTX increased the median survival to 55 d ($p < 0.001$). Compared to the free PTX group, the median survival for the DC-PNM-PTX was 69.5 d ($p = 0.03$).

Discussion

We report the development of bladder cancer-specific targeting micelles that are crosslinked with disulfide bonds to stabilize during blood circulation and coated with PLZ4 bladder cancer-targeting ligand for cancer-specific drug delivery. DC-PNM specifically delivered a higher drug load to patient-derived bladder cancer xenografts than to lung cancer xenografts in the same mice after intravenous administration. At the same dose, DC-PNM-PTX was more effective than free PTX in prolonging the progression-free survival as well as the survival of mice carrying patient-derived xenografts.

Nanomedicine has emerged as promising diagnostic and therapeutic modalities in the management of cancer. However, no such drugs have been approved for bladder cancer [13]. We previously reported the development of non-crosslinked PNM that represents a significant development compared to free PTX in Cremophor EL/ethanol (Taxol®). One major issue associated with PTX is its hydrophobic nature that requires a special solvent Cremophor EL/ethanol. Even with the administration of pre-chemotherapy medications including anti-histamine and steroids, some patients still develop severe allergic and even anaphylactic reactions to PTX in Cremophor EL/ethanol. In order to decrease the toxicity and improve the efficacy, several nanoformulations of PTX have been developed and reported (reviewed in [9]), including polymeric nanoparticles, such as Poly[Lactic-Co-Glycolic Acid] or PLGA, Poly [ε-Caprolactone] or PCL, Poly [L-Lactide] or PLA, chitosan, albumin and gelatin, lipid-based nanoparticles, such as liposome, solid lipid, lipid nanocapsules and emulsion; and PTX-polymer conjugates. However, they have various limitations. For example, the FDA approved PTX albumin nanoformulation Abraxane® has large size (~130 nm) and aggregates within 24–48 h after reconstitution. Some other drawbacks associated with these nanoformulations include the lack of cancer-targeting drug delivery and premature drug release. We previously reported that the formulation of PTX in PNM eliminated the need for Cremophor EL/ethanol, and did not induce mast cell degranulation that may contribute to allergic reactions [6]. However, the mechanical force and lipoproteins in blood circulation can dissolve PNM and prematurely release the drug load. In addition, the PNM-building polymer teloden-drimers work as a detergent and cause hemolysis as they have hydrophobic cholic acid octamers at one end and hydrophilic PEG and PLZ4 at the other end.

To overcome these drawbacks, we developed DC-PNM. This formulation eliminates the need of Cremophor EL/ethanol just as non-crosslinked PNM, and can significantly reduce the risk of allergic reactions. In addition, DC-PNM possesses additional features that non-crosslinked PNM lacks. Disulfide crosslinks can stabilize DC-PNM. Non-crosslinked nanomicelles immediately dissolved after the addition of a strong ionic detergent SDS [5]. Here, we showed that DC-PNM maintained its integrity even in the presence of SDS, suggesting that DC-PNM can withstand the effect of lipoproteins during blood circulation. In our study, DC-PNM only dissolved after the addition of glutathione at the physiological concentration of 10 mM. Consistent with the increased stability, we observed increased half-life of DC-PNM when $T_{1/2\beta}$ increased from 527 to 929 min ($p = 0.037$). In addition, the efficacy of PTX was significantly improved when formulated in DC-PNM. We previously showed that the formulation of PTX in non-crosslinked micelles significantly mitigated the toxicity, but possessed efficacy comparable to that of free PTX. Here, we showed that the efficacy of PTX was further improved with DC-PNM when compared to free PTX (figure 4). Combining all these factors, DC-PNM-PTX

significantly delayed the tumor growth and prolonged the survival of mice carrying patient-derived xengrafts when compared to free PTX in Cremophor EL/ethanol.

The nanoformulation of highly toxic chemotherapeutic agents can significantly reduce toxicity, and achieve increased drug delivery to cancer sites secondary to the enhanced permeability and retention effects. Several clinical trials are already underway to determine the efficacy and toxicity of these agents. The decoration of nanomoieties with cancer-specific targeting ligands can further enhance drug delivery to cancer sites, and potentiate the anti-tumor activity while decreasing non-specific drug delivery to other organs. The disulfide crosslinking of nanoparticles makes on-demand drug delivery into cancer cells possible as crosslinking stabilizes the nanoparticles during blood circulation and releases the drug after the nanoparticles enter into the reducing intracellular environment (with 10 mM glutathione). As the active drug of DC-PNM-PTX is PTX, that is already widely used in clinical bladder cancer treatment with moderate effect, we expect that the nanoformulation can potentially decrease the toxicity, improve the efficacy and improve the treatment outcomes.

In conclusion, DC-PNM-PTX eliminates the need for Cremophor EL/ethanol in formulating PTX, remains intact in the presence of a strong detergent SDS, modifies PTX pharmacokinetics after intravenous administration, improves *in vivo* drug delivery, and enhances the anti-cancer efficacy of PTX. Further investigation is warranted to translate this development into clinical application.

Acknowledgments

This study was supported by the Veteran Administration (VA) Career Development Award-2 (PI: Pan), VA Merit (PI: Pan. Grant #: 1I01BX001784), and the NCI Cancer Center Support Grant (PI: de Vere White, Grant P30 CA093373). The work reported here does not represent the views or opinions of the Department of Veterans Affairs or the United States Government.

References

[1] Bendary L, Khalil S, Shahin A and Nawar N 2011 Intravesical gemcitabine versus bacillus Calmette-Guerin (BCG) in treatment of non-muscle invasive bladder cancer: short term comparative study *Conf. Proc. American Urological Association* **185** e664–5

[2] Deponte M 2013 Glutathione catalysis and the reaction mechanisms of glutathione-dependent enzymes *Biochimica et Biophysica Acta* **1830** 3217–66

[3] Grossman H B *et al* 2003 Neoadjuvant chemotherapy plus cystectomy compared with cystectomy alone for locally advanced bladder cancer *New Engl. J. Med.* **349** 859–66

[4] Li Y, Xiao K, Luo J, Lee J, Pan S and Lam K S 2010 A novel size-tunable nanocarrier system for targeted anticancer drug delivery *J. Control. Release* **144** 314–23

[5] Li Y, Xiao K, Luo J, Xiao W, Lee J S, Gonik A M, Kato J, Dong T A and Lam K S 2011 Well-defined, reversible disulfide cross-linked micelles for on-demand paclitaxel delivery *Biomaterials* **32** 6633–45

[6] Lin T Y, Li Y P, Zhang H, Luo J, Goodwin N, Gao T, White Rde V, Lam K S and Pan C X 2013 Tumor-targeting multifunctional micelles for imaging and chemotherapy of advanced bladder cancer *Nanomedicine* **8** 1239–51

[7] Lin T Y, Zhang H, Luo J, Li Y, Gao T, Lara P N Jr, de Vere White R, Lam K S and Pan C X 2012 Multifunctional targeting micelle nanocarriers with both imaging and therapeutic potential for bladder cancer *Int. J. Nanomed.* **7** 2793–804

[8] Luo J, Xiao K, Li Y, Lee J S, Shi L, Tan Y H, Xing L, Holland Cheng R, Liu G Y and Lam K S 2010 Well-defined, size-tunable, multifunctional micelles for efficient paclitaxel delivery for cancer treatment *Bioconjug. Chem.* **21** 1216–24

[9] Ma P and Mumper R J 2013 Paclitaxel nano-delivery systems: a comprehensive review *J. Nanomed. Nanotechnol.* **4** 1000164

[10] Pan C X *et al* 2015 Development and characterization of bladder cancer patient-derived xenografts for molecularly guided targeted therapy *PloS one* **10** e0134346

[11] Siegel R, Naishadham D and Jemal A 2012 Cancer statistics, 2012 *CA: a Cancer Journal for Clinicians* **62** 10–29

[12] Siegel R L, Miller K D and Jemal A 2016 Cancer statistics, 2016 *CA: a Cancer Journal for Clinicians* **66** 7–30

[13] Tomlinson B, Lin T Y, Dall'Era M and Pan C X 2015 Nanotechnology in bladder cancer: current state of development and clinical practice *Nanomedicine* **10** 1189–201

[14] Tornoe C W, Christensen C and Meldal M 2002 Peptidotriazoles on solid phase: [1,2,3]-triazoles by regiospecific copper(I)-catalyzed 1,3-dipolar cycloadditions of terminal alkynes to azides *J. Org. Chem.* **67** 3057–64

[15] Vaughn D J, Broome C M, Hussain M, Gutheil J C and Markowitz A B 2002 Phase II trial of weekly paclitaxel in patients with previously treated advanced urothelial cancer *J. Clin. Oncol.* **20** 937–40

[16] von der Maase H *et al* 2000 Gemcitabine and cisplatin versus methotrexate, vinblastine, doxorubicin, and cisplatin in advanced or metastatic bladder cancer: results of a large, randomized, multinational, multicenter, phase III study *J. Clin. Oncol.* **18** 3068–77

[17] Xiao K, Luo J, Fowler W L, Li Y, Lee J S, Xing L, Cheng R H, Wang L and Lam K S 2009 A self-assembling nanoparticle for paclitaxel delivery in ovarian cancer *Biomaterials* **30** 6006–16

[18] Yamori T, Sato S, Chikazawa H and Kadota T 1997 Anti-tumor efficacy of paclitaxel against human lung cancer xenografts *Jpn. J. Cancer Res.* **88** 1205–10

[19] Zhang H, Aina O H, Lam K S, de Vere White R, Evans C, Henderson P, Lara P N, Wang X, Bassuk J A and Pan C X 2012 Identification of a bladder cancer-specific ligand using a combinatorial chemistry approach *Urologic Oncol.* **30** 635–45